



HAL
open science

Estimation of frequency-wavenumber diagrams using a physics-based grid-free compressed sensing method

Thomas Paviet-Salomon, Julien Bonnel, Clément Dorffer, Barbara Nicolas, Thierry Chonavel, Dag Tollefsen, David P Knobles, Preston S Wilson, Angélique Drémeau

► To cite this version:

Thomas Paviet-Salomon, Julien Bonnel, Clément Dorffer, Barbara Nicolas, Thierry Chonavel, et al.. Estimation of frequency-wavenumber diagrams using a physics-based grid-free compressed sensing method. IEEE Journal of Oceanic Engineering, 2021, 10.1109/JOE.2021.3109432 . hal-03329874

HAL Id: hal-03329874

<https://hal.science/hal-03329874v1>

Submitted on 31 Aug 2021

HAL is a multi-disciplinary open access archive for the deposit and dissemination of scientific research documents, whether they are published or not. The documents may come from teaching and research institutions in France or abroad, or from public or private research centers.

L'archive ouverte pluridisciplinaire **HAL**, est destinée au dépôt et à la diffusion de documents scientifiques de niveau recherche, publiés ou non, émanant des établissements d'enseignement et de recherche français ou étrangers, des laboratoires publics ou privés.

Estimation of frequency-wavenumber diagrams using a physics-based grid-free compressed sensing method

Thomas Paviet-Salomon, Julien Bonnel *Member, IEEE*, Clément Dorffer, Barbara Nicolas
Member, IEEE, Thierry Chonavel, Dag Tollefsen, David P. Knobles, Preston S. Wilson,
Angélique Drémeau

Abstract

Shallow water propagation can be described using modal theory. For low frequency sources, propagated signals are composed of a few dispersive modes, each of them propagating with its own frequency-dependent wavenumber. Modal estimation, and particularly wavenumber estimation, is of great interest in seabed characterization but classically requires a large and dense horizontal line array (HLA). The compressed sensing (CS) paradigm, which allows one to reduce the number of sensors, has been used to overcome this limitation. However, CS performance is directly linked to the discrete basis used in the process and is known to degrade with basis mismatch. To mitigate this issue, the current paper proposes a physics-based grid-free approach to perform wavenumber estimation using a HLA with a limited number of sensors and a single broadband source. The proposed method has three main features: it starts with a speed correction to prevent wavenumber aliasing (using water sound speed at the array location), it then embeds physical prior (the modal dispersion relation) at the core of the CS framework, followed by a CS grid-free approach. The performance of the method is quantified on simulated data using the Jaccard's distance. The method is then applied successfully on experimental data from the 2017 Seabed Characterization Experiment.

Index Terms

Underwater acoustics, compressed sensing, normal mode propagation, Seabed Characterization Experiment, SBCEX17.

T. Paviet-Salomon, C. Dorffer and A. Dremeau are with Lab-STICC, ENSTA Bretagne, UMR CNRS 6285, Brest, France (e-mail: angelique.dremeau@ensta-bretagne.fr, clement.dorffer@ensta-bretagne.fr, thomas.paviet-salomon@ensta-bretagne.org). J. Bonnel is with the Applied Ocean Physics and Engineering Department, Woods Hole Oceanographic Institution, Woods Hole, Massachusetts 02543, USA (e-mail: jbonnel@whoi.edu). B. Nicolas is with Univ Lyon, INSA-Lyon, UJM-Saint Etienne, CNRS, Inserm, Creatis UMR 5220, U1206, F-69601, Lyon, France. T. Chonavel is with Lab-STICC, IMT Atlantique, UMR CNRS 6285, Brest, France (thierry.chonavel@imt-atlantique.fr). D. Tollefsen is with the Norwegian Defence Research Establishment (FFI), Defence Systems Division, Horten NO-3191, Norway (e-mail: dag.tollefsen@ffi.no). P. Wilson is with The Walker Department of Mechanical Engineering & Applied Research Laboratories, University of Texas at Austin, Austin, Texas 78712, USA (e-mail: pswilson@mail.utexas.edu). D. Knobles is with Knobles Scientific and Analysis, LLC, Austin, Texas 78731, USA (e-mail: dpknobles@kphysics.org)

I. INTRODUCTION

1
2 In shallow-water environments (water depth $D < 200$ m), the acoustic propagation of a low-frequency
3 ($f < 100$ Hz) signal is conveniently described by normal mode theory. Under this assumption, the signal
4 is modeled by the sum of a small number of propagating modes (less than ten in this work). The modes
5 are fully characterized by their frequency-dependent wavenumbers and amplitudes. These two modal
6 features have been extensively used as input data for inverse problems, such as source localization [1],
7 [2] and/or environmental estimation [3], [4]. As a result, modal estimation is an important topic for ocean
8 acoustics. The present paper focuses on modal wavenumber estimation.

9 When range aperture is available, wavenumber estimation is similar to spectral analysis in the spatial
10 dimension. Assuming that the signal is collected on a long horizontal line array (HLA) with a source
11 in the endfire direction, the easiest way to estimate the wavenumber spectrum is to compute a spatial
12 Fourier transform (SFT) in the horizontal dimension. Further, if the source is broadband, one can also
13 compute a second Fourier transform in the temporal dimension (TFT) to obtain a frequency-wavenumber
14 (f-k) diagram, which fully characterizes modal dispersion [5], [6].

15 The main drawback of this simple procedure is that it suffers from the traditional limitations of the
16 Fourier-based spectral analysis. In our context, a large horizontal aperture and a large number of sensors
17 (i.e. a long and dense HLA) are required to properly resolve the modal wavenumbers. To mitigate
18 this issue, the SFT can be replaced by more advanced spectral estimation methods. Pioneer studies
19 successfully replaced the SFT with an auto-regressive (AR) estimator [7], [8]. Since the propagation
20 in shallow-water environments is described by a small number of modes, considering sparse models
21 constitutes an interesting alternative. These models are in particular involved in the compressed sensing
22 (CS) paradigm [9] which, as it will be emphasized in the following, is of particular interest here, but has
23 been more broadly exploited in underwater acoustics (e.g. [10], [11]). CS has first been used to estimate
24 modal wavenumber in ocean acoustics by Le Courtois et al. [12]. Interestingly, CS has also been used to
25 estimate modal wavenumber in other scientific fields, e.g. structural health monitoring using Lamb waves
26 [13], [14]. A special issue of the Journal of The Acoustical Society of America is dedicated to CS in
27 acoustics, and the editorial introduction [15] includes a comprehensive review of CS.

28 Traditionally, CS algorithms expand the signal on the elements of a finite basis, i.e. a discrete grid.
29 When the components of the signal do not match the grid, basis mismatch occurs, which degrades the
30 CS performances [16]. Off-grid CS approaches have been proposed to mitigate this issue [17], [18].
31 They have been notably applied to underwater acoustic problems, such as plane wave beamforming
32 [19] or modal estimation using a vertical line array (VLA) and a source at multiple ranges [20]. Later,

33 Pavier-Salomon et al. [21] proposed to use grid-free CS to perform modal wavenumber estimation using
34 a single broadband source and a small number of sensors. As in Ref. [22], they further embedded a
35 physical assumption, the *dispersion relation*, within the CS framework to relate wavenumbers from one
36 (temporal) frequency to the next. The method was successfully validated on data simulated in a Pekeris
37 waveguide [21].

38 In the present article, we extend the work of Pavier-Salomon et al. [21]. The method is improved by
39 implementing a frequency-dependent shift of the wavenumber spectra. This processing, which effectively
40 creates an equivalent baseband version of the spatial signal thanks to a speed correction, is traditionally
41 used for seismic applications [5], [6]. Here, it prevents wavenumber aliasing and thus allows wavenumber
42 estimation over a relatively wide frequency band. On the other hand it modifies the dispersion relation
43 that is used at the core of the CS framework.

44 In the present work, the performances of the proposed method is benchmarked on realistic simulations,
45 and shown to be superior to the state of the art. The method is also applied on experimental marine data
46 collected during the 2017 Seabed Characterization Experiment (SBCEX17) [23]. This article considers
47 a combusive sound source (CSS) signal recorded on a HLA with an aperture of 1 km. The proposed
48 method allows the estimation of the wavenumbers of the four first modes from 10 Hz to 100 Hz using as
49 few as 10 sensors. These experimental results, obtained on SBCEX17 data collected on the New England
50 Mud Patch, illustrate the method's robustness to complex environments with vertical stratification. Indeed,
51 the New England Mud Patch features a complex layered seafloor. It notably has a layer of mud whose
52 upper part is believed to be slower than water [24], [25], which clearly impacts the propagating modes
53 [26].

54 The remainder of the paper is organized as follows. Section II briefly introduces modal propagation,
55 and focuses on the dispersion relation which will be at the core of the proposed method. Section III
56 reviews the CS framework. It then describes on-grid and off-grid methods. Section IV presents the
57 proposed wavenumber estimation procedure. First, Sec. IV-A reviews speed correction, a process that
58 prevents wavenumber aliasing. Then, Sec. IV-B details the physics-based grid-free wavenumber tracking
59 algorithm. Lastly, Sec IV-C introduces the Jaccard distance, a suitable metric to assess the performances of
60 the method. Applications are presented in Sec. V, which covers a simulated benchmark and comparison
61 with the state-of-the-art, as well as experimental results obtained using data from the 2017 Seabed
62 Characterization Experiment. Section VI summarizes and concludes the article.

II. ACOUSTIC PROPAGATION IN DISPERSIVE SHALLOW WATER ENVIRONMENTS

63

A. Received signal

64

65 This paper focuses on low-frequency ($f < 100$ Hz) acoustic propagation in shallow water ($D < 200$ m).
 66 In this context, as stated in Sec. I, the propagation is described by the modal theory. Consider a frequency-
 67 domain signal $s(f)$ emitted by a source at depth at z_s . The received pressure on a sensor located at the
 68 distance r and depth z can be written as [27, Chap 5]:

$$y(f, r) \simeq Q \frac{s(f)}{\sqrt{r}} \sum_{m=1}^{M(f)} A_m(f, z_s, z) e^{-jr k_{rm}(f)} + n(f, r), \quad (1)$$

69

where Q is a constant factor, $M(f)$ is the number of propagating modes at frequency f , $k_{rm}(f)$ is the
 70 horizontal wavenumber of the m^{th} mode, and $A_m(f, z_s, z)$ is its amplitude. The quantity $n(f, r)$ stands
 71 for the TFFT of the measurement noise. Modal attenuation is usually included in Eq. (1) as the imaginary
 72 part of k_{rm} . Here, the associated term $e^{-r \Im[k_{rm}(f)]}$ is included in A_m , so that k_{rm} can be considered a
 73 real number.

74

We consider a HLA and a source in the endfire direction (i.e. the source is aligned with the array).
 75 The geometrical attenuation factor $1/\sqrt{r}$ in Eq. (1) can be compensated for if the source position is
 76 known. As a result, the only significant range-dependence in Eq. (1) is within the phase of the modes.
 77 Note that this is still a fair assumption even if the source position is unknown, as long as it is in the
 78 endfire direction. Indeed, most of the range variability in Eq. (1) is driven by the complex exponential
 79 $e^{-jr k_{rm}(f)}$, and the $1/\sqrt{r}$ can be considered as constant along the HLA, provided that the source/array
 80 distance is large enough. As a result $y(f, k)$, the SFT of $y(f, r)$, provides a direct measurement of the
 81 wavenumber spectrum (i.e. with peaks at $k_{rm}(f)$). For a broadband source, $y(f, k)$ is called a f-k diagram
 82 [5]. Figure 1 presents a simulated f-k diagram. The simulation has been run for a Pekeris waveguide
 83 representative of a classical shallow water scenario. For consistency, the environmental parameters are
 84 the same as those used in Refs. [21], [22]: water depth $D = 130$ m, sound speed $c_{water} = 1500$ m/s
 85 and density $\rho_{water} = 1$ g/cm³; basement sound speed $c_{bas} = 2000$ m/s and density $\rho_{bas} = 2$ g/cm³. The
 86 f-k diagram was obtained using the FT of data simulated on a long and dense HLA with 240 regularly
 87 spaced sensors, with sensor spacing $\Delta r = 25$ m (the array length is nearly 6 km).

B. Dispersion relation

88

89 In any environment, the horizontal wavenumbers k_{rm} are linked to their vertical counterparts k_{zm} by
 90 the *dispersion relation*. At a given frequency f , this relation is

$$\left(\frac{2\pi f}{c}\right)^2 = k_{rm}(f)^2 + k_{zm}(f)^2, \quad (2)$$

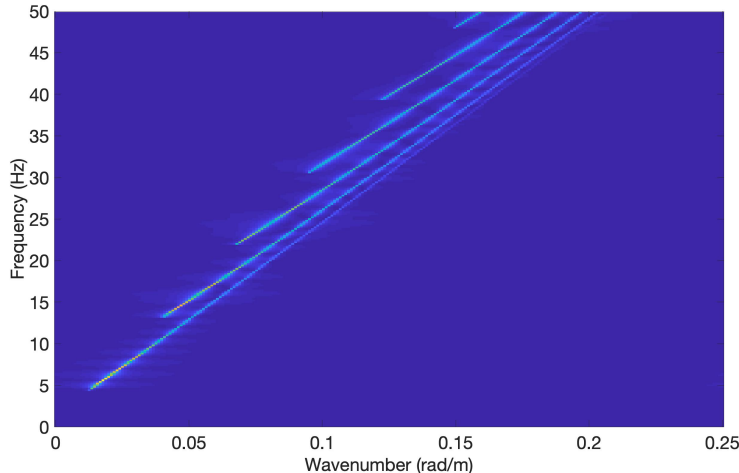


Fig. 1. Simulated f-k diagram in a Pekeris waveguide.

91 where c is the speed of the sound. Note that in theory, both $k_{zm}(f)$ and c are depth dependent. This is
 92 ignored here, as was done in previous studies [21], [22], [28] that use the dispersion relation to guide
 93 modal estimation. Indeed, the potential impact of this assumption is small enough that it can be embedded
 94 into noise and/or other uncertainties.

95 As suggested by Le Courtois and Bonnel [12], one can discretize the frequency axis (with $f = \nu\Delta_f$,
 96 $\nu \in \mathbb{N}$ and Δ_f the size of a frequency bin) and relate the wavenumbers attached to two successive
 97 frequency indices using

$$k_{rm}[\nu + 1]^2 = k_{rm}[\nu]^2 + (2\nu + 1) \left(\frac{2\pi\Delta_f}{c} \right)^2 + \epsilon[\nu], \quad (3)$$

98 where $k_{rm}[\nu] = k_{rm}(\nu\Delta_f)$ and $\epsilon[\nu] = k_{zm}[\nu + 1]^2 - k_{zm}[\nu]^2$.

99 In shallow-water environments, the vertical wavenumbers k_{zm} weakly depend on the frequency [27,
 100 Chap. 5]. As a result, the quantity ϵ is smaller than the other terms of the equation and can be neglected.
 101 This hypothesis has successfully been used in previous studies that took advantage of Eq. (3) at the core
 102 of modal estimation scheme [21], [22], [28]. In the present paper, Eq. (3) will be used as a physical prior
 103 to enhance wavenumber recovery using an off-grid CS algorithm.

104 III. COMPRESSED SENSING

105 A. Sparse representation

106 Using the discretized framework presented in Sec. II-B, we further assume that the received signal
 107 has been measured on a HLA with L elements. The received signal $y(f, r)$ is now denoted using \mathbf{y}_ν , a

108 column vector of size L . Assuming that the horizontal wavenumber space is discretized into a grid of
 109 size N , Eq. (1) can be expressed as

$$\mathbf{y}_\nu = \mathbf{D}\mathbf{a}_\nu + \mathbf{n}_\nu, \quad (4)$$

110 where $\mathbf{D} \in \mathbb{C}^{L \times N}$ is a dictionary made up of (spatial) Fourier component, $\mathbf{a}_\nu \in \mathbb{C}^N$ is the wavenumber
 111 spectrum at the (temporal) frequency ν (i.e. the transposed version of the ν^{th} line of the f-k diagram
 112 of interest) and $\mathbf{n}_\nu \in \mathbb{C}^L$ is the additive noise along the HLA. The $(l, n)^{\text{th}}$ element of \mathbf{D} is defined as
 113 $d_{nl} = e^{-jr_l \kappa_n}$, where r_l is the distance between the l^{th} sensor and the source, and κ_n is the n^{th} element
 114 of the wavenumber search grid. Note that Eq. (4) requires knowledge about the HLA configuration
 115 (i.e. sensor spacing), but does not require the source/array distance to be known, provided that the
 116 source is at the endfire direction. In this case, r_l can be referenced to the first sensor of the HLA (i.e.
 117 $r_1 = 0$). The resulting solution is similar to the one obtained using the absolute source/array distance,
 118 up to a multiplicative phase shift. Note that the n^{th} column of \mathbf{D} will be noted \mathbf{d}_{κ_n} hereinafter, i.e.
 119 $\mathbf{d}_{\kappa_n} = [1, \dots, e^{-jr_L \kappa_n}]^T$.

120 The discrete wavenumber spectrum \mathbf{a}_ν can be estimated through the SFT of \mathbf{y}_ν , which is equivalent to
 121 a least-square estimation process. However, since the number of propagating modes is small, most of the
 122 elements of \mathbf{a}_ν are null. As a result, the use of sparse recovery (SR) is well adapted to estimate \mathbf{a}_ν [12],
 123 [22]. Within this framework, \mathbf{D} is seen as an overcomplete dictionary (i.e. $L \ll N$) while \mathbf{a}_ν contains
 124 many zero entries. The corresponding SR problem can be expressed as

$$\hat{\mathbf{a}}_\nu = \underset{\mathbf{a}_\nu}{\operatorname{argmin}} \|\mathbf{y}_\nu - \mathbf{D}\mathbf{a}_\nu\|_2^2, \text{ subject to } \|\mathbf{a}_\nu\|_0 \leq M_\nu, \quad (5)$$

125 with $\|\mathbf{a}_\nu\|_0$ the l_0 pseudonorm of \mathbf{a}_ν which simply counts the numbers of non-zero entries of \mathbf{a}_ν and
 126 M_ν the maximum number of modes expected to propagate at frequency ν .

127 B. On-grid CS algorithm

128 Eq. (5) is a combinatorial problem, and many heuristic methods have been developed to solve it.
 129 They can roughly be divided into three families. A first group of methods replaces the l_0 -norm by a
 130 l_p -norm (with $0 < p \leq 1$). This leads to a relaxed problem which can be solved efficiently by standard
 131 optimization procedures. A well-known approach is the Basis Pursuit (BP) [29]. A second group of
 132 methods are greedy algorithms which build up the sparse vector \mathbf{a}_ν from successive greedy decisions.
 133 One of the most popular versions of such algorithms is Orthogonal Matching Pursuit (OMP) [30]. The
 134 last group of methods are Bayesian algorithms that express the sparse representation as the solution of
 135 a Bayesian inference problem. Different Bayesian methods consider different prior models, estimation
 136 problems and statistical tools to solve them [31], [32].

137 Various on-grid CS methods have been used to estimate wavenumbers in ocean acoustics, including an
 138 iterative reweighted least squares method [12] and two Bayesian approaches [22], [28]. Interestingly, the
 139 two Bayesian approaches [22], [28] use the dispersion relation Eq. (3) to connect horizontal wavenumbers
 140 from one frequency to the next. However, Ref. [28] assumes that the number of modes is constant over
 141 the bandwidth of interest and that the $\epsilon[\nu]$ term in Eq. (3) can be fully neglected. These two assumptions
 142 restrict the modal recovery to a limited bandwidth (in Ref. [28], the provided examples were limited to
 143 a 20 Hz bandwidth, which kept the number of modes constant). On the other hand, Ref. [22] also uses
 144 Eq. (3) with $\epsilon[\nu] = 0$ to predict wavenumber at frequency $\nu + 1$, but it introduces freedom around
 145 the predictions to account for $\epsilon[\nu] \neq 0$. The associated drawback is that the method includes several
 146 parameters that must be tuned by hand.

147 In the present article, we consider an off-grid CS method that also relies on the dispersion relation
 148 Eq. (3). We will later see that the proposed method enables tracking the wavenumbers over a relatively
 149 wide bandwidth, while the number of modes does not need to be known *a priori*. Before that, traditional
 150 off-grid CS is briefly presented.

151 C. Off-grid CS algorithm

152 On-grid CS methods have known limitations that notably occur when the non-zero coefficients of \mathbf{a}_ν
 153 do not match the grid points. This issue, called basis-mismatch [33], [16], can be mitigated by using a
 154 very fine grid. However, this raises questions about the coherence of the grid (which in turns impacts
 155 CS performance) and also may induce numerical instabilities.

156 These concerns led to the development of grid-free setting methods. Practically, a grid-free version
 157 of the relaxed version of Eq. (5) can be obtained by replacing the l_1 norm (only valid in a finite
 158 dimensional setting) by the total variation norm [34]. Although the underlying theory is complex, off-
 159 the-shelf toolboxes such as the CVX software (ConVeX: a library for convex optimization) [35] are
 160 available to solve the problem. This approach was notably used to estimate wavenumbers (and modal
 161 depth functions) considering a VLA and a source at multiple ranges [20]. However, the main drawback
 162 of this procedure is its high computational cost.

163 Simultaneously, a continuous version of OMP has been proposed in Ref. [17] while a continuous
 164 version of BP has been proposed in Ref. [36]. The approach is based on the idea of interpolating the
 165 dictionary components in between existing grid points. However, an expensive computational cost is still
 166 associated with those methods. Rather, we will use a traditional OMP method, coupled with gradient
 167 descent performed after each OMP step [37]. The main advantage of this method is to obtain a continuous
 168 behavior while being simple, it barely increases the computational cost of the considered SR method. It

169 was previously used in our context (estimation of modal wavenumbers with a HLA) on data simulated
 170 in a Pekeris waveguide [21].

171 IV. WAVENUMBER ESTIMATION

172 This section describes the proposed method to estimate modal wavenumbers. A modified dispersion
 173 relation that will be used within the CS framework is first presented.

174 A. Dispersion relation after speed correction

175 In any waveguide, the modal wavenumbers are known to be contained within the interval $[\frac{2\pi f}{c_{\max}}, \frac{2\pi f}{c_{\min}}]$,
 176 where c_{\max} and c_{\min} are the maximal and minimal sound speed in the environment [27, Chap. 5]. At any
 177 frequency, the wavenumber support of the signal is limited to a relatively narrow (wavenumber) band:
 178 the spatial signal is said to be a bandpass signal. A small sensor spacing is thus required to prevent
 179 wavenumber aliasing. An example of an aliased f-k diagram is presented in Fig. 2a. The simulated
 180 environment is the same as in Fig. 1, except that the frequency now goes up to 200 Hz. One can see
 181 that above 60 Hz, wavenumbers are aliased. This is because for $f > 60$ Hz, the maximal wavenumber
 182 value $\frac{2\pi f}{c_{\min}}$ is above the (spatial) Nyquist frequency $k_s = \frac{1}{2\Delta r}$, with Δr the (spatial) sampling rate (i.e.
 183 the sensor spacing).

184 Aliasing can be prevented by reducing the spacing between sensors, but this is not always possible at
 185 sea. Since the wavenumber spectrum is a bandpass signal, aliasing can also be prevented by translating
 186 the modal spectrum toward smaller wavenumber (i.e. baseband processing). Mathematically, this is done
 187 by time-shifting the received data using c_{\min} sound speed, which in the frequency domain corresponds
 188 to

$$\tilde{y}(f, r) = e^{(jr \frac{2\pi f}{c_{\min}})} y(f, r), \quad (6)$$

189 with $\tilde{y}(f, r)$ the shifted signal. The wavenumber support of \tilde{y} becomes $[\frac{2\pi f}{c_{\max}} - \frac{2\pi f}{c_{\min}}, 0]$, which drastically
 190 reduces the Nyquist frequency. This process is common in geophysics [5], [38], [39] and has also found
 191 applications in ocean acoustics [6], [40]. It will be called speed correction hereafter. Speed correction
 192 is applied on the simulated Pekeris example, and the result is presented in Fig. 2b. One can see that
 193 wavenumbers can now be recovered without aliasing up to 200 Hz.

194 Although the speed correction process is simple, it modifies the dispersion relation. The original
 195 wavenumbers $k_{rm}[\nu]$ and their shifted versions $\tilde{k}_{rm}[\nu]$ are linked through

$$k_{rm}[\nu] = \tilde{k}_{rm}[\nu] + \gamma\nu, \quad (7)$$

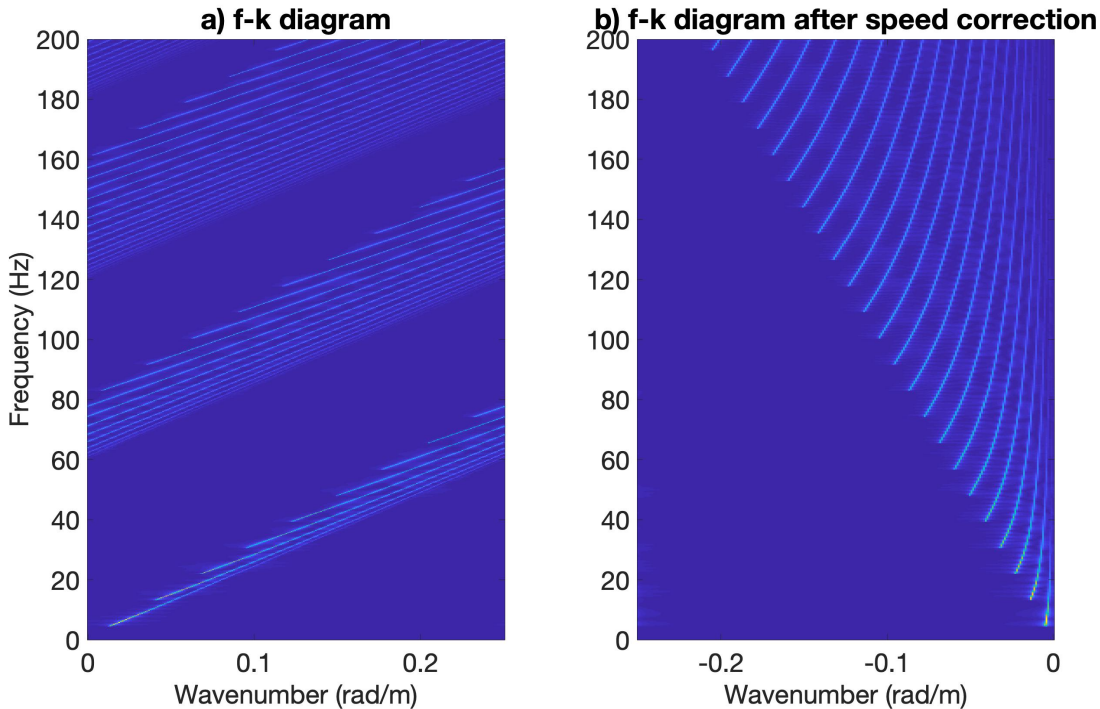


Fig. 2. a) : Frequency-wavevector diagram in the same configuration as in Fig. 1, except that frequency goes to 200 Hz: wavenumber are aliased for $f > 60$ Hz. b) : f-k diagram in the same configuration, but after speed correction: there is no aliasing.

196 with $\gamma = \frac{2\pi\Delta_f}{c_{\min}}$. Using Eq. (7) into Eq. (3), the discretized dispersion relation becomes

$$(\tilde{k}_{rm}[\nu + 1] + \gamma(\nu + 1))^2 = (\tilde{k}_{rm}[\nu] + \gamma\nu)^2 + (2\nu + 1)\gamma^2 + \epsilon[\nu]. \quad (8)$$

197 Assuming that $\epsilon[\nu] = 0$, the wavenumber at frequency $\nu + 1$ can be predicted using

$$\tilde{k}_{rm}^{\text{pred}}[\nu + 1] = -\gamma(\nu + 1) + \sqrt{(\tilde{k}_{rm}[\nu] + \gamma\nu)^2 + (2\nu + 1)\gamma^2}. \quad (9)$$

198 Note that in the proposed method, the (incorrect) assumption $\epsilon[\nu] = 0$ will be mitigated by looking for
199 wavenumbers in a small interval centered around the predicted value $\tilde{k}_{rm}^{\text{pred}}[\nu + 1]$.

200 B. Tracking modes

201 As stated in the introduction, the tracking method proposed in this article is largely similar to the one
202 in Ref. [21]. The only difference is that we now work after speed correction. As a result, the physical
203 prior that is embedded into the grid-free CS algorithm is now Eq. (8), instead of Eq. (3). This enables
204 tracking wavenumbers in configurations where sensor spacing is large and creates wavenumber aliasing.
205 In such situation, the method from Ref. [21] cannot be used. Note that if sensor spacing is small enough

206 to prevent aliasing without speed correction, then the proposed method gives result similar to the method
 207 in Ref. [21]. The proposed method is summarized below.

208 The proposed procedure starts at $\nu = 1$ with a traditional OMP step, evaluating the most correlated
 209 atom of the dictionary \mathbf{D} with the signal \mathbf{y}_ν . This step is then completed by a detection operation, which
 210 compares the resulting correlation to a given threshold T_0 . If selected, a mode is considered to propagate
 211 and the dispersion relation (8) is used to predict the interval in which the wavenumber of this mode is
 212 likely to be at the next frequency. The current estimate, as well as the predicted wavenumber at the next
 213 frequency, are then refined by a gradient-descent step, respectively based on the selected atom and within
 214 the predicted interval. For the predicted wavenumber of mode m at the next frequency $\nu + 1$, a detection
 215 threshold $T_{m,\nu+1}$ is again applied on its estimated amplitude to prevent the propagation of false alarms.
 216 All these steps are then repeated at the next frequency in order to detect possible new modes and to
 217 propagate those already predicted to higher frequencies.

218 The overall procedure is summarized in the Algorithm 1. An important parameter is ξ in Eq. (11): it
 219 gives the algorithm freedom to look for $\tilde{k}_{rm}[\nu + 1]$ around the predicted value $\tilde{k}_{rm}^{\text{pred}}[\nu + 1]$. In a given
 220 context, the value of ξ is empirically determined by simulations to maximize the method's performances.

Algorithm 1 Physics-based grid-free Orthogonal Matching Pursuit for data with speed correction.

0. Initialization : $\forall \nu \in \{1, \dots, F\}$, $\mathbf{r}_\nu = \mathbf{y}_\nu$, $\mathcal{S}_\nu = \emptyset$, $I_{0,\nu} = \emptyset$, $M = 0$.

For $\nu = 1 : F$

1. Find new propagating wavenumber

$$\hat{\kappa}_n = \underset{\kappa_n}{\operatorname{argmax}} |\langle \mathbf{r}_\nu, \tilde{\mathbf{d}}_{\kappa_n} \rangle|, \quad (10)$$

where $\tilde{\mathbf{d}}_{\kappa_n}$ is the n -th column of $\mathbf{D}_{\cup_{m \in \{0, \dots, M\}} I_{m,\nu}}$ made up of Fourier atoms not in $\cup_{m \in \{0, \dots, M\}} I_{m,\nu}$.

If $|\langle \mathbf{r}_\nu, \tilde{\mathbf{d}}_{\hat{\kappa}_n} \rangle| \geq T_0$

– Set $M = M + 1$.

– Apply gradient-descent algorithm to refine previous estimate and get $\hat{k}_{rm}[\nu]$. Set $\mathcal{S}_\nu = \mathcal{S}_\nu \cup \hat{k}_{rm}[\nu]$.

– Compute corresponding coefficients and update residual : $\mathbf{r}_\nu = \mathbf{y}_\nu - \mathbf{D}_{\mathcal{S}_\nu} \hat{\mathbf{a}}_{\nu, \mathcal{S}_\nu}$ with $\hat{\mathbf{a}}_{\nu, \mathcal{S}_\nu} = \mathbf{D}_{\mathcal{S}_\nu}^+ \mathbf{y}_\nu$, with $\mathbf{D}_{\mathcal{S}_\nu}^+$ the Moore-Penrose pseudo-inverse matrix of $\mathbf{D}_{\mathcal{S}_\nu}$, dictionary made up of Fourier atoms specified by \mathcal{S}_ν .

2. If $M > 1$, propagate existing modes

For $m = 1 : M - 1$

– Apply gradient-descent on interval $I_{m,\nu}$ and get $\hat{k}_{rm}[\nu]$. If $|\langle \mathbf{r}_\nu, \mathbf{d}_{\hat{k}_{rm}[\nu]} \rangle| \geq T_{m,\nu}$, set $\mathcal{S}_\nu = \mathcal{S}_\nu \cup \hat{k}_{rm}[\nu]$.

– Compute corresponding coefficients and update residual : $\mathbf{r}_\nu = \mathbf{y}_\nu - \mathbf{D}_{\mathcal{S}_\nu} \hat{\mathbf{a}}_{\nu, \mathcal{S}_\nu}$ with $\hat{\mathbf{a}}_{\nu, \mathcal{S}_\nu} = \mathbf{D}_{\mathcal{S}_\nu}^+ \mathbf{y}_\nu$.

3. Predict propagating intervals for next frequency

For all $m \in \{1, \dots, M\}$, define

$$I_{m,\nu+1} = [\tilde{k}_{rm}^{\text{pred}}[\nu + 1] - \xi; \tilde{k}_{rm}^{\text{pred}}[\nu + 1] + \xi]. \quad (11)$$

221 Detection thresholds may depend on false alarm probabilities. More particularly, considering a Gaussian
 222 complex circular noise assumption with variance σ^2 , we can define T_0 as

$$T_0 = \sigma \sqrt{-2 \log \beta_0} \quad (12)$$

223 where β_0 is a given false alarm probability considered for the detection of a new mode. We adopt a
 224 similar definition for $T_{m,\nu}$, but we add further physical considerations. If a mode m is detected first at
 225 frequency $\nu_{c,m}$ with threshold T_0 , we know that the mode will still be present at higher frequencies,
 226 suggesting thus to decrease the threshold for increasing frequencies. This can be done by considering:

$$T_{m,\nu} = T_0 - \sum_{i=1}^{\nu-\nu_{c,m}} \left(\frac{1 - \frac{T_\infty}{T_0}}{2 - \frac{T_\infty}{T_0}} \right)^i T_0, \quad (13)$$

227 where $T_\infty = \sigma\sqrt{-2\log\beta_\infty}$ stands for a desired limit threshold depending on an asymptotic false alarm
 228 probability β_∞ under the same Gaussian complex circular noise assumption. More details on the adopted
 229 strategy with regard to these thresholds can be found in [21].

230 C. Performance of the algorithm : the Jaccard distance

231 An interesting question arises in quantifying the performance of the proposed method. Since the mode
 232 number is not known *a priori*, it is important to account for mismatch between the estimated number of
 233 modes, the true number of modes, and the fact that this number may vary with frequency. As a result, the
 234 problem can be seen as the detection and tracking of an unknown number of targets. A relevant metric
 235 in this context is the Jaccard distance [18], [41], [42].

236 The Jaccard distance D_J is built using traditional detection theory features: the true positive (TP), false
 237 negative (FN) and false positive (FP) rates. Here, the quantities TP, FN and FP are evaluated at every
 238 frequency of interest using an acceptance radius R_J . To explain the definition of TP, FN and FP, let us
 239 assume that we have a theoretical wavenumber $k_{rm}^{theo}[\nu]$ and an estimated wavenumber $\hat{k}_r[\nu]$:

- 240 • if $[k_{rm}^{theo}[\nu] - R_J, k_{rm}^{theo}[\nu] + R_J]$ contains a single estimated mode $\hat{k}_r[\nu]$, then $\hat{k}_r[\nu]$ is a TP;
- 241 • if $[k_{rm}^{theo}[\nu] - R_J, k_{rm}^{theo}[\nu] + R_J]$ contains several estimated modes, then the closest $\hat{k}_r[\nu]$ from $k_{rm}^{theo}[\nu]$
 242 is a TP while the others are FP (it is implicitly assumed that R_J is smaller than half of the smallest
 243 distance between all theoretical modes, i.e. the acceptance radii do not intercept);
- 244 • if there is no estimated mode $\hat{k}_r[\nu]$ such that $|k_{rm}^{theo}[\nu] - \hat{k}_r[\nu]| \leq R_J$ then $k_{rm}^{theo}[\nu]$ is a FN.

245 Mathematically, the Jaccard's index J_I is first defined

$$J_I = \frac{\text{TP}}{\text{TP} + \text{FP} + \text{FN}} \quad (14)$$

246 and leads to the definition of the Jaccard distance

$$D_J = 1 - J_I \quad (15)$$

247 which is such that $0 < D_J < 1$. Note that $D_J = 0$ means that $\text{TP} = 1$ and $\text{FP} = \text{FN} = 0$. On the other
 248 hand $D_J = 1$ means that $\text{TP} = 0$, while $D_J \gg 0$ means that FP and/or FN are much larger than TP.

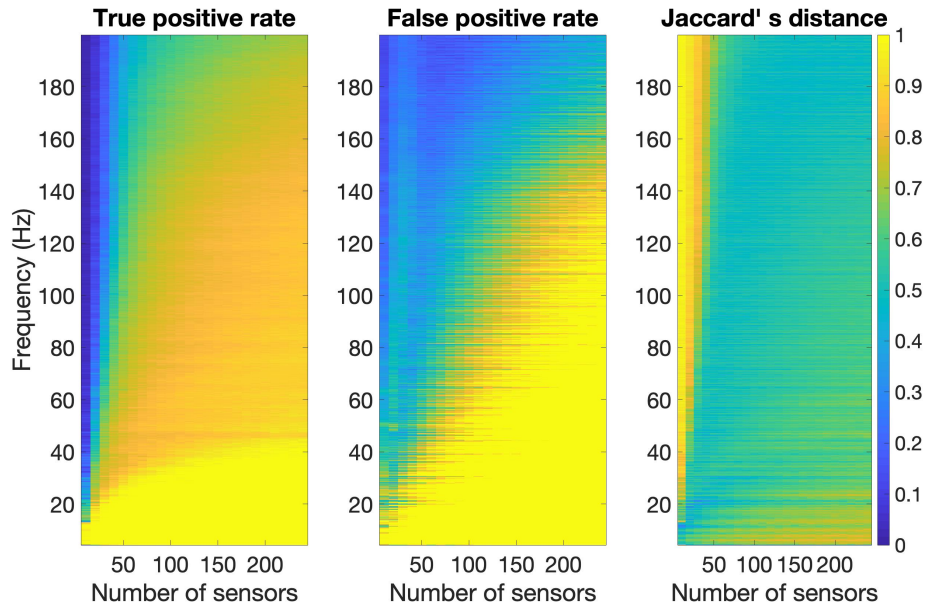


Fig. 3. Performance of the estimation of modal wavenumbers in a simulated Pekeris waveguide using OMP: TP (left), FP (middle) and D_J (right).

249 The relevance of the Jaccard distance is illustrated using data simulated in our Pekeris waveguide
 250 example. For the sake of simplicity, wavenumbers are estimated using a classical OMP method. OMP is
 251 an iterative algorithm, selecting a new wavenumber at each iteration. Two stopping criteria are classically
 252 considered for this algorithm: it can stop either when the estimated reconstruction error drops below a
 253 given threshold or when the number of non-zero coefficients achieves a given number. This latter criterion
 254 is very convenient in our context, because the number of iterations is equivalent to the number of modes
 255 to be recovered. Although practical, this requires accurate prior information about the number of modes
 256 at each frequency. On the other hand, the stopping criterion based on the energy of the residual is less
 257 demanding in terms of prior information. This criterion is similar to what is used in the proposed method.
 258 It will thus be used to illustrate the interest of the Jaccard distance.

259 Estimation performance is illustrated in Fig. 3. The TP rate increases when the number of sensors
 260 increases (because more data makes the estimation easier), and increases when the frequency decreases
 261 (because modal density decreases which also facilitates the estimation). On the other hand, the FP rate is
 262 high at very low frequencies (because the number of modes is very low, and thus a single false positive
 263 drastically increases the FP rate). The FP rate also tends to increase with the number of sensors. This is
 264 due to the chosen stopping criterion which implies an increasing number of iterations in OMP, and thus
 265 increases the likeliness to make false positive mistakes.

Overall, the Jaccard distance D_J is consistent with the behavior of TP and FP. As an example, D_J is high (estimation performance is poor) when TP is small (e.g. for small number of sensors) and/or when FP is high (e.g. at very low frequencies). Also, when the sensor number is large enough, D_J is relatively constant, because TP and FP tend to compensate for each other. The Jaccard distance is thus a good metric to summarize global estimation performance and will be used in the following.

V. APPLICATION

In this section, the performance of the method is assessed on realistic simulations. The method is also applied on experimental marine data collected during the 2017 Seabed Characterization Experiment (SBCEX17). The considered applications focuses on low-frequency data ($f < 100$ Hz). In our context, this makes the number of modes relatively small (5 or less), which allows for modal estimation with a small number of sensors. This choice is consistent (and allows comparison) with previous modal estimation studies based on sparsity [12], [22], [28].

This section starts with a description of SBCEX17, whose context will be used to define the simulated environment.

A. SBCEX17

The SBCEX17 was dedicated to the understanding of sound propagation in fine-grained sediment. It was a multi-year, multi-institutional and multi-disciplinary effort which took place on the New England Mud Patch (NEMP). The NEMP is located about 100 km south of Cape Cod. The area is characterized by a relatively flat bathymetry (water depth $D \sim 70\text{--}75$ m) and a thick upper sediment layer of mud.

A preliminary environmental survey was conducted in 2015. It notably included an intensive coring effort, as well as a high-resolution seismic survey. The main experiment took place in March-April 2017. It involved three research vessels, and many acoustic sources and receivers were deployed, covering frequencies from ~ 10 Hz to 10 kHz. A previous special issue of the IEEE Journal of Oceanic Engineering is dedicated to SBCEX17. Its editorial introduction [23] provides a succinct overview of SBCEX17.

B. Experimental context

The SBCEX data was collected on a long HLA (aperture ~ 1 km). The considered source is a Combustive Sound Source deployed at 18:38 UTC on March 18 2017 at CSS station 29, located at (40.4983N, 70.5842W). The source signal is a powerful broadband impulse followed by several secondary impulses called bubble pulses [43]. Note that here, the specific source waveform does not matter as long as the source signal to noise ratio (SNR) is good enough in the frequency band of interest. The

receiving system is a 64 element HLA with a horizontal aperture of 1016 m deployed by the Norwegian Defence Research Establishment (FFI). The array orientation was roughly West-East, and the positions of the hydrophones at the HLA extremities are (40.4984N, 70.4677W) and (40.4983N, 70.4557W). The hydrophone spacing along the array is not uniform. The array elements have approximately logarithmic spacing (from 0.8 m to 72 m), with a symmetry around the array center and a higher density in the middle of the array. The specific source/array configuration has been chosen so that the source is in the endfire direction, and the distance between the source and the HLA is about 10 km. Note that in this context, the range variability along the HLA induced by the $1/\sqrt{r}$ term in Eq. (1) is negligible and can be ignored.

C. Simulation framework

First, the performance of the method is assessed using simulated data that mimics the experimental context. The environment is modeled using results from an inversion study performed using the HLA data [44]. The environment is modeled as follows:

- water column: depth $D = 65$ m, sound speed gradient from 1468 m/s at the top of the layer to 1469 m/s at the bottom;
- sediment layer: thickness $h = 5$ m, sound speed $c_{\text{sed}} = 1500$ m/s, density $\rho_{\text{sed}} = 1.6$ g/cm³, attenuation $\alpha_{\text{sed}} = 0.1$ dB/ λ ;
- basement: $c_{\text{bas}} = 1700$ m/s, density $\rho_{\text{bas}} = 2.0$ g/cm³, attenuation $\alpha_{\text{sed}} = 0.2$ dB/ λ .

Acoustic propagation is simulated in this environment over 0-100 Hz using the normal mode code ORCA [45] with a frequency bin size of **XX** Hz, which led to simulation of **YY** frequencies. The environmental impulse response along the array is simulated in the range-frequency domain for a source at $r = 10$ km in the endfire direction. The array configuration mimics the experimental geometry. A bi-dimensional (2D) Gaussian white noise is added to the impulse response in the range-frequency domain, and the signal to noise ratio (SNR) is evaluated as the power of the (2D) range-frequency impulse response divided by the power of the (2D) range-frequency noise. Speed correction (see Sec. IV-A) is then applied with $c_{\text{min}} = 1468$ m/s. Finally, f-k diagrams are computed using four different methods:

- 1) OMP: a traditional OMP algorithm;
- 2) SoBaP: a soft Bayesian Pursuit method that uses the dispersion relation to relate wavenumbers from one frequency to the next [22];
- 3) COMP: a grid-free OMP algorithm that uses gradient descent (COMP: Continuous OMP);
- 4) CPOMP: the method proposed in this article (CPOMP: Continuous and Physics-based OMP, i.e. which uses the dispersion relation).

328 The methods OMP, SoBaP and COMP have been chosen as representative of the state-of-the-art. Note
 329 that OMP and COMP have been implemented here using the mode number as a stopping criterion (i.e. at
 330 frequency f , each algorithm looks for $M(f)$ wavenumbers). This gives them a strong advantage over the
 331 proposed method, which automatically determines the mode number. For CPOMP, we set $\beta_0 = 0.001$,
 332 $\beta_\infty = 0.5$ and $\xi = 10^{-3}$.

333 Beside, all the methods considered here rely on the construction of the dictionary \mathbf{D} (see Sec.III-A).
 334 To construct this dictionary, one needs to sample the wavenumber axis with N elements. This is done
 335 by choosing a grid size and a maximum wavenumber value of interest. The grid size is defined as one
 336 fifth of the smallest value between 2 propagating modes over the frequency band of interest. Further,
 337 the maximum wavenumber value is computed considering the Nyquist theorem applied to the maximum
 338 space between two consecutive sensor (here $\Delta_k = 5.10^{-4}$ rad/m and $\kappa_n = -0.09$ rad/m).

339 *D. Performance study*

340 A first set of simulations studies the impact of the number of sensors on the f-k diagram estimation
 341 for a given SNR (12 dB). For a given number of sensors, sensors are randomly selected, except for the
 342 two sensors at the extremities of the HLA which are always selected (these two sensors are on both ends
 343 of the HLA so that total aperture of the array is always the same). The obtained performance is shown
 344 in Fig. 4 for 2 different frequency bands: 0–50 Hz and 50–100 Hz. Clearly, performance increases with
 345 number of sensors for all the methods, and the proposed method (CPOMP) outperforms the state of the
 346 art. Performance gain is minimal in the 0–50 Hz band, because most methods (OMP, COMP, CPOMP)
 347 provide satisfactory results. However, at higher frequencies where more modes are propagating, the gains
 348 of the proposed method becomes evident, for all number of sensors. As an example, with 40 sensors,
 349 CPOMP has $D_J < 0.1$. This corresponds to an excellent f-k diagram recovery, as is illustrated at the end
 350 of this subsection. Interestingly, SoBaP which is supposed to be the most advanced of the state-of-the-art
 351 methods is the one with the worst performance. This is because SoBaP has been developed for data
 352 without speed correction. Although the SoBaP dispersion relation has been modified here to take into
 353 account the corrected dispersion relation, this is clearly not enough to correctly track wavenumbers. It is
 354 likely possible to further modify SoBaP to regain performance, but this is beyond the present scope.

355 A second set of simulations studies the impact of SNR for a given number of sensors (32), and for
 356 SNR from 0 dB to 12 dB. Again, for a given simulation, sensor selection is random but for the HLA
 357 extremities which are always used. Results are shown in Fig. 5. Performance naturally increases as SNR
 358 increases for all the methods. Once again, CPOMP outperforms all the other methods, and SoBaP exhibits
 359 poor performance. In particular, CPOMP provides very satisfactory f-k reconstruction ($D_J < 0.1$) for

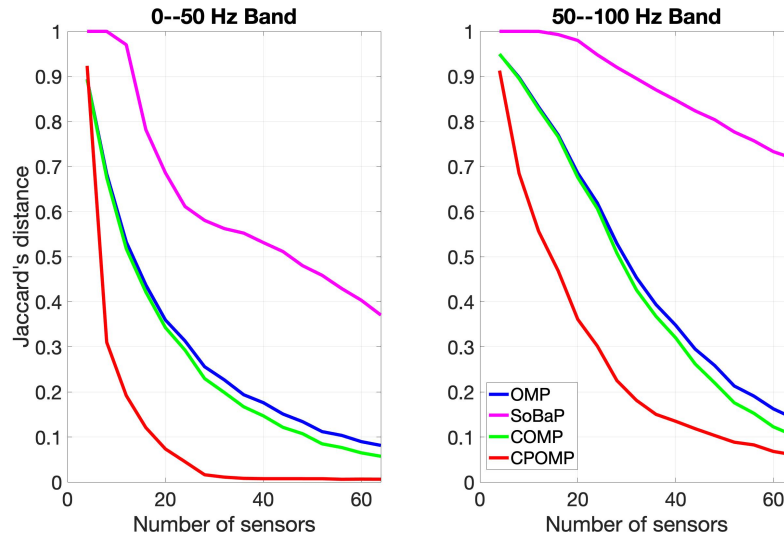


Fig. 4. Jaccard's distance as a function of the number of sensors for a SNR of 12 dB.

360 SNR > 5 dB. Also, both in Figs. 4 and 5, the performance gain of COMP with respect to OMP is
 361 relatively small, while the performance gain of CPOMP with respect to COMP is more significant. This
 362 demonstrates the importance of including physics (the dispersion relation) at the core of any grid-free
 363 CS method.

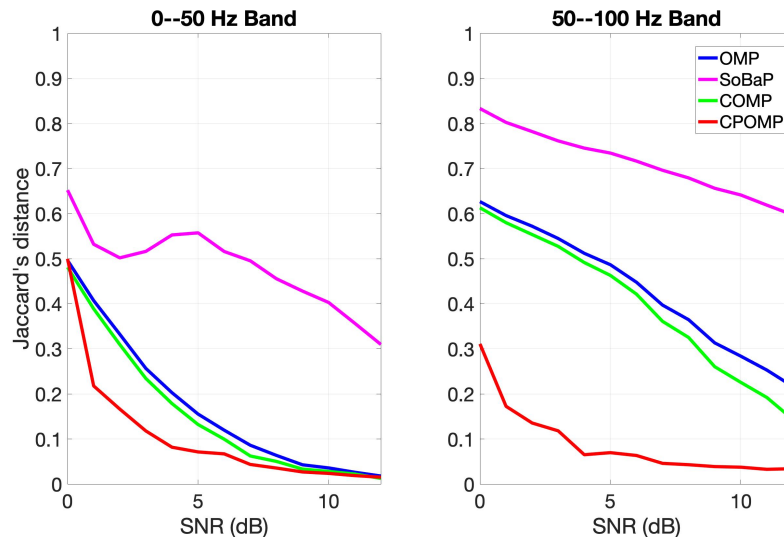


Fig. 5. Jaccard's distance as a function of the SNR - using 32 sensors

364 The Jaccard distance D_J study fully characterizes the performance of the four methods. However, it is

365 difficult to relate a specific D_J value to an actual wavenumber tracking result. To mitigate this issue, an
 366 example of wavenumber tracking with 40 sensors and SNR = 12 dB is illustrated in Fig. 6. It is clear
 367 that in this configuration, CPOMP performs really well ($D_J = 0.04$). OMP ($D_J = 0.13$) and COMP
 368 ($D_J = 0.13$) also perform well, although they make a substantial number of false alarms. On the other
 369 hand, SoBaP ($D_J = 0.71$) suffers from false alarms and missed detections, which explains its poor D_J
 370 value.

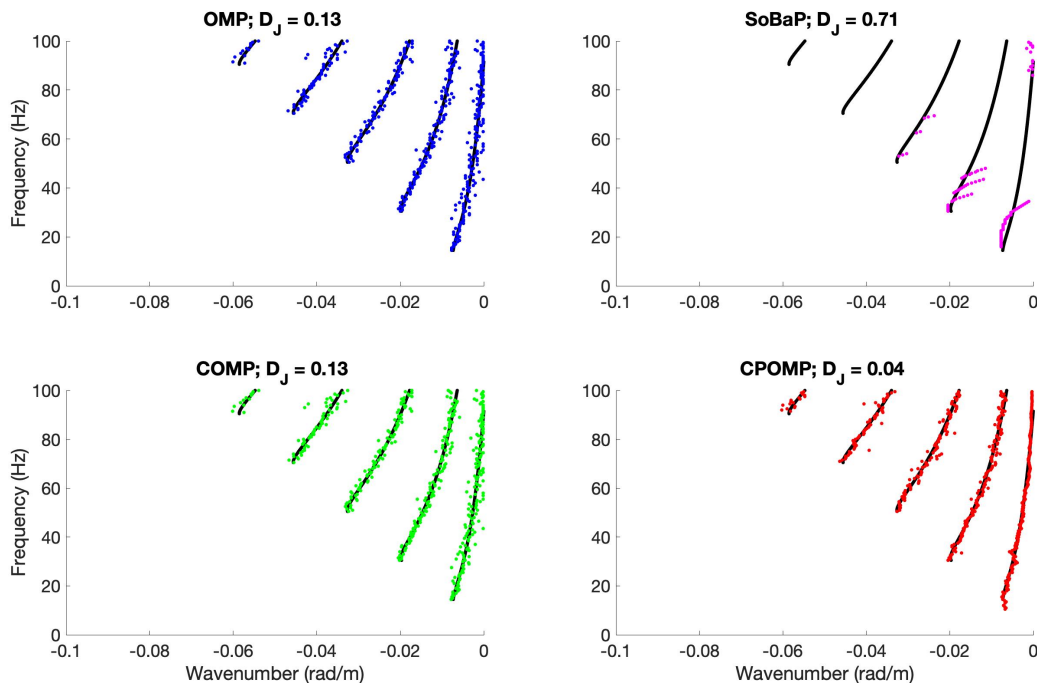


Fig. 6. Wavenumber estimation on simulated data with 40 sensors and a SNR of 12 dB. Black: true wavenumbers ; blue: OMP, magenta: SoBaP, green: COMP, red: CPOMP.

371 E. Experimental results

372 The proposed method is now applied to the experimental CSS data described in Sec. V-B. Speed
 373 correction is first applied on the data using $c_{\min} = 1459$ m/s, a value empirically determined to time-
 374 align the data along the array. Wavenumber estimation is then performed using CPOMP and COMP.
 375 The objective here is to exclusively compare the proposed method (CPOMP) to the best method of the
 376 state-of-the-art (COMP).

377 Wavenumbers are estimated using 10, 40 and 64 sensors. Experimental results are presented in Fig. 7.
 378 Since no perfect ground truth is available to assess the experimental performance, the CPOMP 64-sensor

379 estimation is used as a reference (black dots in Fig. 7) to visually evaluate the results. One can see that
 380 CPOMP is consistently better than COMP. With 40 sensors, CPOMP gives results that are comparable to
 381 the 64-sensor reference. This is consistent with the simulated study which shows that CPOMP performance
 382 is roughly constant between 40 and 64 sensors (see Fig. 4). Interestingly, CPOMP also provides a good
 383 wavenumber estimation using only 10 sensors, although the last mode is missed. On the other hand, the
 384 COMP estimation with 10 sensors suffers from the small number of sensors, which leads to a consequent
 385 number of false alarms.

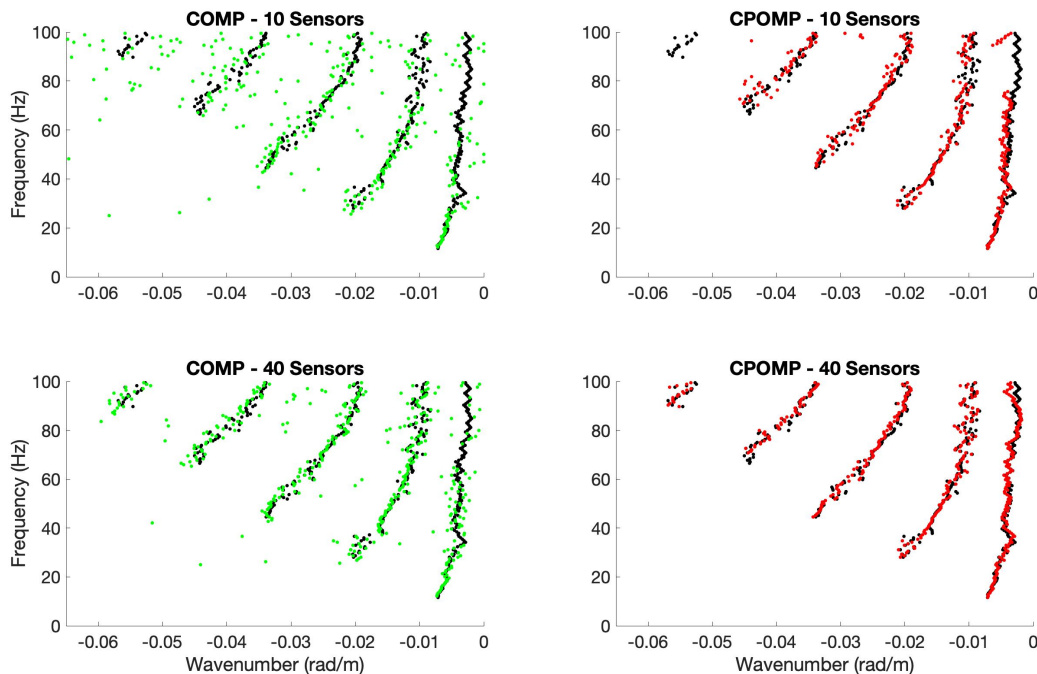


Fig. 7. (black) Recovery of CPOMP with 64 sensors, (green) recovery with COMP, (red) recovery with CPOMP

386 VI. CONCLUSION

387 The article presents a physics-based grid-free CS method to estimate modal wavenumber using a
 388 broadband source and a HLA with a small number of sensors. The method is based on three ideas. First
 389 of all, the method benefits from speed correction, so that a range-frequency signal can be conveniently
 390 sampled without wavenumber aliasing. Second, the method uses a grid-free framework to mitigate known
 391 CS drawbacks associated with basis mismatch. Last but not least, the method embeds physical information
 392 within the CS framework: it uses the dispersion relation (compensated for speed correction) to relate
 393 wavenumbers from one frequency to the other.

394 The proposed method has been benchmarked on simulations using the Jaccard distance as a performance
395 metric. It was demonstrated that the method outperforms the state-of-the-art. Further, the method is
396 experimentally validated on experimental data collected during SBCEX17. It notably allows a good
397 estimation of modal wavenumbers from 0 to 100 Hz using as few as 10 sensors.

398 Although the proposed method works with a small number of sensors, it still requires a large horizontal
399 aperture. As a result, a potential application for the method is modal estimation using synthetic aperture,
400 as obtained using a fixed receiver and a moving source. This context is particularly appealing for
401 geoaoustic inversion, where estimated modal wavenumbers can be used as an input to estimate the
402 seafloor geoaoustic properties [8], [46]. Following the CS paradigm, the proposed method can be used
403 to collect fewer samples, but better ones. This has practical consequences for ocean acoustics, since the
404 production of man-made source signal underwater is now considered as pollution [47]. Reducing the
405 number of samples (which is equivalent to the number of source signals in a synthetic aperture context)
406 is an important perspective to reduce the noise footprint of ocean acoustic experiments.

407 ACKNOWLEDGMENT

408 This work was supported by the Delegation Generale de L'Armement (DGA), the Office of Naval
409 Research (ONR), the ONR Global, the LABEX CeLyA (ANR-10-LABX-0060) of Université de Lyon,
410 within the program "Investissements d'Avenir" (ANR-16-IDEX-0005) operated by the French National
411 Research Agency (ANR).

REFERENCES

- 412
- 413 [1] G. R. Wilson, R. A. Koch, and P. J. Vidmar, "Matched mode localization," *The Journal of the Acoustical Society of*
414 *America*, vol. 84, no. 1, pp. 310–320, 1988.
- 415 [2] Y. Le Gall, F.-X. Socheleau, and J. Bonnel, "Performance analysis of single-receiver matched-mode localization," *IEEE*
416 *Journal of Oceanic Engineering*, vol. 44, no. 1, pp. 193–206, 2017.
- 417 [3] G. V. Frisk and J. F. Lynch, "Shallow water waveguide characterization using the Hankel transform," *The Journal of the*
418 *Acoustical Society of America*, vol. 76, no. 1, pp. 205–216, 1984.
- 419 [4] M. S. Ballard and K. M. Becker, "Inversion for range-dependent water column sound speed profiles on the New Jersey shelf
420 using a linearized perturbative method," *The Journal of the Acoustical Society of America*, vol. 127, no. 6, pp. 3411–3421,
421 2010.
- 422 [5] Ö. Yilmaz, *Seismic data analysis: Processing, inversion, and interpretation of seismic data*, ch. 1–2. No. 10, Society of
423 Exploration Geophysicists (Tulsa), 2001.
- 424 [6] B. Nicolas, J. Mars, and J.-L. Lacoume, "Geoacoustical parameters estimation with impulsive and boat-noise sources,"
425 *IEEE Journal of Oceanic Engineering*, vol. 28, no. 3, pp. 494–501, 2003.
- 426 [7] K. M. Becker and G. V. Frisk, "Evaluation of an autoregressive spectral estimator for modal wave number estimation in
427 range-dependent shallow water waveguides," *The Journal of the Acoustical Society of America*, vol. 120, no. 3, pp. 1423–
428 1434, 2006.
- 429 [8] M. S. Ballard, K. M. Becker, and J. A. Goff, "Geoacoustic inversion for the New Jersey shelf: 3-D sediment model," *IEEE*
430 *Journal of Oceanic Engineering*, vol. 35, no. 1, pp. 28–42, 2010.
- 431 [9] E. J. Candès and M. B. Wakin, "An introduction to compressive sampling," *IEEE Signal Processing Magazine*, vol. 25,
432 no. 2, pp. 21–30, 2008.
- 433 [10] N. Chapman and I. Barrodale, "Deconvolution of marine seismic data using the l_1 norm," *Geophysical Journal International*,
434 vol. 72, no. 1, pp. 93–100, 1983.
- 435 [11] P. Gerstoft, A. Xenaki, and C. F. Mecklenbräuker, "Single and multiple snapshot compressive beamforming," *arXiv preprint*
436 *arXiv:1503.02339*, 2015.
- 437 [12] F. Le Courtois and J. Bonnel, "Compressed sensing for wideband wavenumber tracking in dispersive shallow water," *The*
438 *Journal of the Acoustical Society of America*, vol. 138, no. 2, pp. 575–583, 2015.
- 439 [13] J. B. Harley and J. M. Moura, "Dispersion curve recovery with orthogonal matching pursuit," *The Journal of the Acoustical*
440 *Society of America*, vol. 137, no. 1, pp. EL1–EL7, 2015.
- 441 [14] S. Sabeti, C. A. Leckey, L. De Marchi, and J. B. Harley, "Sparse wavenumber recovery and prediction of anisotropic
442 guided waves in composites: a comparative study," *IEEE Transactions on Ultrasonics, Ferroelectrics, and Frequency*
443 *Control*, vol. 66, no. 8, pp. 1352–1363, 2019.
- 444 [15] P. Gerstoft, C. Mecklenbräuker, W. Seong, and M. Bianco, "Introduction to special issue on compressive sensing in
445 acoustics.," *The Journal of the Acoustical Society of America*, vol. 143, no. 6, pp. 3731–3731, 2018.
- 446 [16] M. F. Duarte and R. G. Baraniuk, "Spectral compressive sensing," *Applied and Computational Harmonic Analysis*, vol. 35,
447 no. 1, pp. 111–129, 2013.
- 448 [17] K. C. Knudson, J. Yates, A. Huk, and J. W. Pillow, "Inferring sparse representations of continuous signals with continuous
449 orthogonal matching pursuit," in *Advances in Neural Information Processing Systems*, pp. 1215–1223, 2014.
- 450 [18] Q. Denoyelle, *Theoretical and Numerical Analysis of Super-Resolution Without Grid*. PhD thesis, Paris Sciences et Lettres,
451 2018.

- 452 [19] A. Xenaki and P. Gerstoft, “Grid-free compressive beamforming,” *The Journal of the Acoustical Society of America*,
453 vol. 137, no. 4, pp. 1923–1935, 2015.
- 454 [20] Y. Park, P. Gerstoft, and W. Seong, “Grid-free compressive mode extraction,” *The Journal of the Acoustical Society of*
455 *America*, vol. 145, no. 3, pp. 1427–1442, 2019.
- 456 [21] T. Paviet-Salomon, C. Dorffer, J. Bonnel, B. Nicolas, T. Chonavel, and A. Drémeau, “Dispersive grid-free orthogonal
457 matching pursuit for modal estimation in ocean acoustics,” in *ICASSP 2020-2020 IEEE International Conference on*
458 *Acoustics, Speech and Signal Processing (ICASSP)*, pp. 4602–4606, IEEE, 2020.
- 459 [22] A. Drémeau, F. Le Courtois, and J. Bonnel, “Reconstruction of dispersion curves in the frequency-wavenumber domain
460 using compressed sensing on a random array,” *IEEE Journal of Oceanic Engineering*, vol. 42, no. 4, pp. 914–922, 2017.
- 461 [23] P. S. Wilson, D. P. Knobles, and T. B. Neilsen, “Guest editorial an overview of the seabed characterization experiment,”
462 *IEEE Journal of Oceanic Engineering*, vol. 45, no. 1, pp. 1–13, 2020.
- 463 [24] J. Belcourt, C. W. Holland, S. E. Dosso, J. Dettmer, and J. A. Goff, “Depth-dependent geoacoustic inferences with dispersion
464 at the new england mud patch via reflection coefficient inversion,” *IEEE Journal of Oceanic Engineering*, vol. 45, no. 1,
465 pp. 69–91, 2019.
- 466 [25] M. S. Ballard, K. M. Lee, A. R. McNeese, P. S. Wilson, J. D. Chaytor, J. A. Goff, and A. H. Reed, “In situ measurements
467 of compressional wave speed during gravity coring operations in the new england mud patch,” *IEEE Journal of Oceanic*
468 *Engineering*, vol. 45, no. 1, pp. 26–38, 2019.
- 469 [26] J. Bonnel, S. Dosso, J. Goff, Y. Lin, J. Miller, G. Potty, P. Wilson, and D. Knobles, “Trans-dimensional geoacoustic
470 inversion using prior information on range-dependent seabed layering,” *IEEE Journal of Oceanic Engineering*, 2021. in
471 press (DOI: 10.1109/JOE.2021.3062719).
- 472 [27] F. B. Jensen, W. A. Kuperman, M. B. Porter, and H. Schmidt, *Computational Ocean Acoustics*, ch. 5,10. Springer Science
473 & Business Media, 2011.
- 474 [28] H. Niu, P. Gerstoft, E. Ozanich, Z. Li, R. Zhang, Z. Gong, and H. Wang, “Block sparse bayesian learning for broadband
475 mode extraction in shallow water from a vertical array,” *The Journal of the Acoustical Society of America*, vol. 147, no. 6,
476 pp. 3729–3739, 2020.
- 477 [29] S. S. Chen, D. L. Donoho, and M. A. Saunders, “Atomic decomposition by basis pursuit,” *SIAM review*, vol. 43, no. 1,
478 pp. 129–159, 2001.
- 479 [30] Y. C. Pati, R. Rezaifar, and P. S. Krishnaprasad, “Orthogonal matching pursuit: Recursive function approximation with
480 applications to wavelet decomposition,” in *Proceedings of 27th Asilomar Conference on Signals, Systems and Computers*,
481 pp. 40–44, IEEE, 1993.
- 482 [31] B. A. Olshausen and D. J. Field, “Sparse coding with an overcomplete basis set: A strategy employed by v1?,” *Vision*
483 *Research*, vol. 37, no. 23, pp. 3311–3325, 1997.
- 484 [32] C. Fevotte and S. J. Godsill, “A bayesian approach for blind separation of sparse sources,” *IEEE Transactions on Audio,*
485 *Speech, and Language Processing*, vol. 14, no. 6, pp. 2174–2188, 2006.
- 486 [33] Y. Chi, L. L. Scharf, A. Pezeshki, and A. R. Calderbank, “Sensitivity to basis mismatch in compressed sensing,” *IEEE*
487 *Transactions on Signal Processing*, vol. 59, no. 5, pp. 2182–2195, 2011.
- 488 [34] E. J. Candès and C. Fernandez-Granda, “Towards a mathematical theory of super-resolution,” *Communications on Pure*
489 *and Applied Mathematics*, vol. 67, no. 6, pp. 906–956, 2014.
- 490 [35] M. Grant and S. Boyd, “CVX: Matlab software for disciplined convex programming, version 2.1,” 2014.
- 491 [36] C. Ekanadham, D. Tranchina, and E. P. Simoncelli, “Recovery of sparse translation-invariant signals with continuous basis
492 pursuit,” *IEEE Transactions on Signal Processing*, vol. 59, no. 10, pp. 4735–4744, 2011.

- 493 [37] P. Chen, Z. Cao, Z. Chen, and C. Yu, "Sparse off-grid doa estimation method with unknown mutual coupling effect,"
494 *Digital Signal Processing*, vol. 90, pp. 1–9, 2019.
- 495 [38] S. L. Freire and T. J. Ulrich, "Application of singular value decomposition to vertical seismic profiling," *Geophysics*,
496 vol. 53, no. 6, pp. 778–785, 1988.
- 497 [39] G. Duncan and G. Beresford, "Median filter behaviour with seismic data 1," *Geophysical Prospecting*, vol. 43, no. 3,
498 pp. 329–345, 1995.
- 499 [40] M. Nardin, F. Glangeaud, and D. Mauuary, "1-200 Hz wave propagation in shallow water," in *IEEE Oceanic Engineering*
500 *Society. OCEANS'98. Conference Proceedings (Cat. No. 98CH36259)*, vol. 1, pp. 390–394, IEEE, 1998.
- 501 [41] P. Jaccard, "Étude comparative de la distribution florale dans une portion des alpes et des jura," *Bull Soc Vaudoise Sci Nat*,
502 vol. 37, pp. 547–579, 1901.
- 503 [42] J. C. Gower and M. J. Warrens, "Similarity, dissimilarity, and distance, measures of," *Wiley StatsRef: Statistics Reference*
504 *Online*, pp. 1–11, 2014.
- 505 [43] A. R. McNeese, P. S. Wilson, J. D. Sagers, and D. P. Knobles, "An impulsive source with variable output and stable
506 bandwidth for underwater acoustic experiments," *The Journal of the Acoustical Society of America*, vol. 136, no. 1,
507 pp. EL8–EL12, 2014.
- 508 [44] D. Tollefsen, S. E. Dosso, and D. P. Knobles, "Ship-of-opportunity noise inversions for geoacoustic profiles of a layered
509 mud-sand seabed," *IEEE Journal of Oceanic Engineering*, vol. 45, no. 1, pp. 189–200, 2019.
- 510 [45] E. K. Westwood, C. T. Tindle, and N. R. Chapman, "A normal mode model for acousto-elastic ocean environments," *The*
511 *Journal of the Acoustical Society of America*, vol. 100, no. 6, pp. 3631–3645, 1996.
- 512 [46] G. V. Frisk, K. M. Becker, S. D. Rajan, C. J. Sellers, K. Von Der Heydt, C. M. Smith, and M. S. Ballard, "Modal mapping
513 experiment and geoacoustic inversion using sonobuoys," *IEEE Journal of Oceanic Engineering*, vol. 40, no. 3, pp. 607–620,
514 2014.
- 515 [47] C. M. Duarte, L. Chapuis, S. P. Collin, D. P. Costa, R. P. Devassy, V. M. Eguiluz, C. Erbe, T. A. Gordon, B. S. Halpern,
516 H. R. Harding, *et al.*, "The soundscape of the anthropocene ocean," *Science*, vol. 371, no. 6529, 2021.